REPORT DOCUMENTATION PAGE

Form Approved
OMB No. 0704-0188

PLEASE DO NOT RETURN YOUR FORM TO THE ABOVE ORGANIZATION.

1. REPORT DATE *(DD-MM-YYYY)*	2. REPORT TYPE	3. DATES COVERED *(From - To)*
11-05-2015	Conference Proceedings	

4. TITLE AND SUBTITLE

Distributed Compressive Sensing vs. Dynamic Compressive Sensing: Improving the Compressive Line Sensing Imaging System through Their Integration

5a. CONTRACT NUMBER

5b. GRANT NUMBER

5c. PROGRAM ELEMENT NUMBER

0602435N

6. AUTHOR(S)

Bing Ouyang, Weilin Hou, Frank M. Caimi, Fraser R. Dalgleish, Anni K. Vuorenkoski, Sue Gong

5d. PROJECT NUMBER

5e. TASK NUMBER

5f. WORK UNIT NUMBER

73-6504-04-5

7. PERFORMING ORGANIZATION NAME(S) AND ADDRESS(ES)

Naval Research Laboratory
Oceanography Division
Stennis Space Center, MS 39529-5004

8. PERFORMING ORGANIZATION REPORT NUMBER

NRL/PP/7330--15-2547

9. SPONSORING/MONITORING AGENCY NAME(S) AND ADDRESS(ES)

Office of Naval Research
One Liberty Center
875 North Randolph Street, Suite 1425
Arlington, VA 22203-1995

10. SPONSOR/MONITOR'S ACRONYM(S)

ONR

11. SPONSOR/MONITOR'S REPORT NUMBER(S)

12. DISTRIBUTION/AVAILABILITY STATEMENT

Approved for public release, distribution is unlimited.

13. SUPPLEMENTARY NOTES

14. ABSTRACT

In recent years, a compressive sensing based underwater imaging system has been under investigation: the Compressive Line Sensing (CLS) imaging system. In the CLS system, each line segment is sensed independently; with regard to signal reconstruction, the correlation among the adjacent lines is exploited via the joint sparsity in the distributed compressive sensing model. Interestingly, the dynamic compressive sensing signal model is also capable of exploiting the correlated nature of the adjacent lines through a Bayesian framework. This paper proposes a new CLS reconstruction technique through the integration of these different models, and includes an evaluation of the proposed technique using the experiment dataset obtained from an underwater imaging test setup.

15. SUBJECT TERMS

Compressive Line Sensing (CLS) imaging system; underwater imaging system

16. SECURITY CLASSIFICATION OF:			17. LIMITATION OF ABSTRACT	18. NUMBER OF PAGES	19a. NAME OF RESPONSIBLE PERSON
a. REPORT	b. ABSTRACT	c. THIS PAGE			Weilin Hou
Unclassified	Unclassified	Unclassified	UU	12	19b. TELEPHONE NUMBER *(Include area code)* (228) 688-5257

Reset

PUBLICATION OR PRESENTATION RELEASE REQUEST

15-1231-1189

Pubkey: 9630

NRLINST 5510.40

1. REFERENCES AND ENCLOSURES

Ref: (a) NRL Instruction 5600.2
(b) NRL Instruction 5510.40E

Encl: (1) Two copies of subject publication/presentation

URGENT

2. TYPE OF PUBLICATION OR PRESENTATION

( ) Abstract only, published	( ) Abstract only, not published
( ) Book author	( ) Book chapter
( ) Book editor	( ) Multimedia report
(X) Conference Proceedings (refereed)	( ) Conference Proceedings (not refereed)
( ) Journal article (refereed)	( ) Journal article (not refereed)
( ) Oral Presentation, published	( ) Oral Presentation, not published
( ) Video ( ) Poster	( ) Other, explain

ALL DOCUMENTS/PRESENTATIONS MUST BE ATTACHE

3. ADMINISTRATIVE INFORMATION

STRN NRL/PP/7330-15-2547
Route Sheet No. 7330/
Job Order No. 73-6604-04-5
Classification U S C
FOUO
Sponsor ONR BASE 6.2-R1
Sponsor's approval yes* (attached)
(*Required if research is otheran 6.1/6.2 NRL or ONR unclassifind research or if publication/presentation is classifed

4. AUTHOR

Title of Paper or Presentation

Distributed Compressive Sensing vs. Dynamic Compressive Sensing: Improving the Compressive Line Sensing Imaging System through their Integration

AUTHOR(s) LEGAL NAMES(s) OF RECORD (First, MI, Last), CODE, (Affiliation if not NRL).

Bing Ouyang Florida Atlantic Univ., Weilin Hou 7333, Frank Caimi Florida State Univ., F.R. Dalgleish Florida Atlantic Univ., Anni Vuorenskoski Florida Atlantic University, Sue Gong Texas Christian Univ.,

This paper will be presented at the SPIE DSS
(Name of Conference)

20-APR - 24-APR-15, Baltimore, MD, Unclassified
(Date, Place and Classification of Conference)

and/or for published in SPIE DSS, Unclassified
(Name and Classification of Publication) (Name of Publisher)

5. CERTIFICATION OR CLASSIFICATION

It is my opinion that the subject paper (is ____) (is not __x__) classified, in accordance with reference (b) and this paper does not violate any disclosure of trade secrets or suggestions of outside individuals or concerns which have been communicated to the NRL in confidence.

This subject paper (has ____) (has never __x__) been incorporated in an official NRL Report.

Weilin Hou, 7333 (Signature)
Name and Code (Principal Author) (Legal Name of Record and Signature Only)

6. ROUTING/APPROVAL (NOTE: If name other than your legal name of record is annotated on the publication or presentation itself, add an explanatory note in the "comments" section below next to your signed legal name of record).

CODE	SIGNATURE	DATE	COMMENTS
Co-Author(s) Weilin Hou, 7333		4/13/15	Need by 20 Apr 2015
Section Head			This is a Final Security Review. Any changes made in the document, after approved by Code 1231, nullify the Security Review.
Branch Head Richard L. Crout, 7330		4-13-2015	
Division Head Ruth H. Preller, 7300		4/13/15	1. To the best knowledge of this Division, the subject matter of this publication (has ____)(has never ____ Xbeen classified 2. This paper (does ____) (does not __X__) contain any militarily critical technology.
ADOR/Director NCST E. R. Franchi, 7000			
DOR/CO			
Security, Code 1231		4/14/15	A copy of the paper, abstract or presentation is filed in this office.
Associate Counsel,Code 1008.3	invention memo	5-8-2015	
Public Affairs (Unclassified/ Unlimited Only), Code 7030.4		4-17-15	
Division, Code			
Author, Code			

HQ-NRL 5511/6 (Rev. 12/14) THIS FORM CANCELS AND SUPERSEDES ALL PREVIOUS VERSIONS

Distributed Compressive Sensing vs. Dynamic Compressive Sensing: Improving the Compressive Line Sensing Imaging System through Their Integration

Bing Ouyang*[1], Weilin Hou[2], Frank M. Caimi[1], Fraser R. Dalgleish[1], Anni K. Vuorenkoski[1], Sue Gong[3]

1. Harbor Branch Oceanographic Institute, Florida Atlantic University, 5600 US1 North, Fort Pierce, FL, USA 34946
2. Naval Research Lab,1005 Balch Blvd, Stennis Space Center, MS 39556
3. Department of Engineering, Texas Christian University, 2800 S University Dr., Fort Worth, TX 76129

*Tel. 772-242-2288, E-mail bouyang@hboi.fau.edu

ABSTRACT

In recent years, a compressive sensing based underwater imaging system has been under investigation: the Compressive Line Sensing (CLS) imaging system. In the CLS system, each line segment is sensed independently; with regard to signal reconstruction, the correlation among the adjacent lines is exploited via the joint sparsity in the distributed compressive sensing model. Interestingly, the dynamic compressive sensing signal model is also capable of exploiting the correlated nature of the adjacent lines through a Bayesian framework. This paper proposes a new CLS reconstruction technique through the integration of these different models, and includes an evaluation of the proposed technique using the experiment dataset obtained from an underwater imaging test setup.

1. BACKGROUND

The laser line scanner (LLS) is state-of-art underwater active imaging technology [6]. The LLS system employs serial raster scan image formation and is compatible with the push-broom type image acquisition commonly used in many survey operations. While the LLS system provides high photon efficiency and narrow instantaneous field of view that are critical for operating in degraded visual environment, the non-adaptive serial raster scan image formation can be a concern in certain situations. For example, higher repetition laser will be required with increased platform speed to maintain the same image spatial resolution, which inevitably will increase the system cost and require more sophisticated noise mitigation. For unmanned platforms such as UAVs and AUVs where power is at a premium, another concern is that the LLS sensor may consume significant power acquiring *redundant* data that will be *discarded* during the image compression phase (Figure 1).

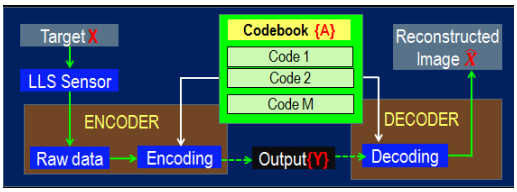

Figure 1. Traditional image acquisition paradigm in a LLS system [3]

The compressive line sensing (CLS) imaging system has been developed [1] to address these concerns. By adopting the concept of resource compression, this system aims to achieve faster signal formation, more flexible system configuration and higher energy efficiency. The technique also enables compact and robust system design. A series of test-tank experiments were conducted to validate the CLS concept [3], and while the results demonstrated the effectiveness of the underlying distributed compressive sensing (DCS) signal model was demonstrated in [3], there was still room for improvements in signal reconstruction process. In this paper we describe our attempt to improve the performance of the CLS system by integrating the "dynamic" compressive sensing concept into the signal reconstruction.

We provide some theoretical foundations in Section 2 and then introduce the CLS concept in Section 3. In Section 4 we introduce the new signal reconstruction technique through the integration of distributed compressive sensing and

Ocean Sensing and Monitoring VII, edited by Weilin W. Hou, Robert A. Arnone, Proc. of SPIE Vol. 9459
94590D · © 2015 SPIE · CCC code: 0277-786X/15/$18 · doi: 10.1117/12.2180130

dynamic compressive sensing signal models. In Section 5 we apply this technique to some test-tank datasets and provide results and detailed analysis. Our conclusions are summarized in Section 6.

.

2. CS AND DCS THEORIES

Compressive sensing (CS) is a framework for the *simultaneous sampling and compression* of sparse signals using incomplete linear measurements [5, 9]. A *K*-sparse signal $\boldsymbol{X} \in R^{N\times 1}$ (i.e., the projection of **X** on a sparsifying basis $\Psi \in R^{N\times N}$:$\boldsymbol{X} = \Psi\boldsymbol{\alpha}$ contains $K \ll N$ non-zero entries) can be recovered with overwhelming probability using more than $M = O(K \log N)$ incoherent linear measurements: $\boldsymbol{y} = \mathrm{A}\boldsymbol{X} = \mathrm{A}\Psi\boldsymbol{\alpha}$ **,** when the measurement matrix $A \in R^{M\times N}$ is incoherent with the sparsifying basis Ψ and satisfies the *Restricted Isometry Property* (RIP) [5]. The vector α (therefore *X*) can be recovered from the measurements *y* by solving an *L1*-minimization problem. Random bases such as Gaussian and Bernoulli are common measurement matrices that satisfy the RIP constraint. For natural signals, the Fourier, discrete cosine transform or wavelet domains are sparsifying bases commonly used in various image/video compression standards and codecs.

The CS theory essentially exploits the intra-signal redundancy within a single source, and, there has been significant interest in extending it to cope with the inter-source correlations. We briefly introduce two such approaches herein. One idea is based on the distributed compressive sensing concept, which we abbreviate as DCS[a]. The other school of thoughts includes modified compressive sensing residual (Lu et al. [14]) and dynamic compressive sensing (Ziniel and Schniter [18]), we abbreviate these techniques as DCS[b].

DCS[a] is closely related to the distributed source coding theorems (Slepian and Wolf [15] and Wyner and Ziv [17]), which hold that the minimum rate of encoding statistically dependent sources independently is the same as the minimum rate of encoding them jointly, when the sources are decoded jointly and their differences are Gaussian.

.

DCS[a] attempts to exploit the inter-signal redundancy among distributed and correlated sources through the establishment of the proper joint sparsity models (JSMs) [4]. In JSM-1 is framework adopted in the CLS framework, all sources $\boldsymbol{X}_l$ within the group consist of a sum of a common component $\boldsymbol{Z}_c$ and a component that is unique to each source Z_l: $\boldsymbol{X}_l = \boldsymbol{Z}_c + \boldsymbol{Z}_l,\ l = 0,1 \ldots L$, where L is the number of signals to be solved jointly. On a sparsifying basis Ψ, $\boldsymbol{Z}_c$ and $\boldsymbol{Z}_l$ can be expressed as $\boldsymbol{Z}_c = \Psi\boldsymbol{\alpha}_c$, $\|\boldsymbol{\alpha}_c\|_0 = K_c$, and $\boldsymbol{Z}_l = \Psi\boldsymbol{\alpha}_l$, $\|\boldsymbol{\alpha}_l\|_0 = K_l$ and both are sparse, i.e., $K_c \ll N$ and $K_l \ll N$. The matrix form of the measurement model is illustrated below:

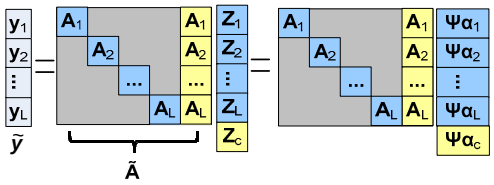

(1)

where $\tilde{\boldsymbol{y}} = [\boldsymbol{y}(1), \ldots, \boldsymbol{y}(L)]^T \in R^{LM\times 1}$ are the measurements of *L* sources within the group; $\tilde{\boldsymbol{\alpha}} = [\boldsymbol{\alpha}(1), \ldots, \boldsymbol{\alpha}(L)]^T \in R^{LN\times 1}$ are the coefficients of the sources on the sparsifying basis Ψ, and $\tilde{A}$ is the measurement matrix. Solving such JSM-1 problem can be casted as *L1* minimization with the cost function formulated by revising Equation (1) [4]:

$$\begin{aligned} &\tilde{\boldsymbol{\alpha}}^* = \arg\min \|\boldsymbol{\alpha}_c\|_1 + \|\boldsymbol{\alpha}_1\|_1 + \cdots + \|\boldsymbol{\alpha}_L\|_1 \\ &\text{subject to } \|\tilde{\boldsymbol{y}} - \tilde{\mathrm{A}}\Psi\tilde{\boldsymbol{\alpha}}\|_2 \le \mathcal{E} \end{aligned} \tag{2}$$

where $\|\boldsymbol{\alpha}_l\|_1 = \sum_{i=1}^{N} |a_l(i)|$ is the *L1*-norm of $\boldsymbol{\alpha}_l$.

DCS[b] formulates a group of correlated sources as recursively reconstructing time sequences of sparse spatial signals. With regard to the measurement acquisition, DCS[a] and DCS[b] are identical – in that each source is measured

independently. With regard to the signal reconstruction, both DCS[a] and DCS[b] assume there is a common component among the different sources. The key difference is that DCS[b] uses the knowledge of the source at the previous time instant as a–priori to increase the sparsity of the signal at current time instant. As a result, the signal reconstruction performance is improved.

There are two approaches in DCS[b] - modified-CS-residual [14] and dynamic CS [18]. In modified-CS-residual, the support estimate $\{S\}$ from the previous time instant will be used as the known part of the support. Then at the current time instant, the scheme attempts to solve the signal that satisfies the data constraint and whose support contains the smallest number of new additions to the known support $\{T\}$ [14]. The scheme can be described by Equation (3) [14]:

$$\begin{aligned} \tilde{\boldsymbol{\alpha}}_{\boldsymbol{p}}^{*} &= \arg\min \gamma\left\|(\boldsymbol{a})_{S_{t-1}^{c}}\right\|_{1} + \left\|\tilde{\boldsymbol{y}}_{\boldsymbol{t,res}} - \mathrm{A}\Psi\boldsymbol{a}\right\|_{2} \\ \tilde{\boldsymbol{\alpha}}_{\boldsymbol{t}} &= \tilde{\boldsymbol{\alpha}}_{\boldsymbol{t,temp}} + \tilde{\boldsymbol{\alpha}}_{\boldsymbol{p}} \end{aligned} \tag{3}$$

where $\tilde{\boldsymbol{y}}_{\boldsymbol{t,res}} = \boldsymbol{y}_{\boldsymbol{t}} - \mathrm{A}\Psi\tilde{\boldsymbol{\alpha}}_{\boldsymbol{t,temp}}$, $\tilde{\boldsymbol{\alpha}}_{\boldsymbol{t,temp}}$ is constructed using support from step t-1 $\boldsymbol{S_{t-1}}$: $\tilde{\boldsymbol{\alpha}}_{\boldsymbol{t,temp}} = (\boldsymbol{a_{t-1}})_{\boldsymbol{S_{t-1}}}$.

In Ziniel and Schniter [18], the dynamic CS adopts a slight different approach. One of the main motivations was to tackle the Bayesian inference high-dimensional problems in a computationally efficient manner. A probabilistic dynamic CS signal model that captures both amplitude and support correlation structure was proposed:

$$\boldsymbol{a_t^n} = \boldsymbol{s_t^n}\boldsymbol{\theta_t^n} \tag{4}$$

where $\boldsymbol{a_t^n}$ represents $\boldsymbol{n^{th}}$ coefficient at time instant $\boldsymbol{t}$, $\{\boldsymbol{s}\}_{\boldsymbol{t=1}}^{\boldsymbol{T}}$ and $\{\boldsymbol{\theta}\}_{\boldsymbol{t=1}}^{\boldsymbol{T}}$ are two hidden random processes and T is the duration of the time sequence. The binary vector $\{\boldsymbol{s}\}$ describes the support of $\{\boldsymbol{a}\}$. $\{\boldsymbol{\theta}\}$ follows normal distribution to describe the amplitudes of the active elements of $\{\boldsymbol{a}\}$. One critical aspect of this algorithm is to update $\{\boldsymbol{a_t}\}$ and to propagate the updates to the next time instant efficiently. A novel approximate message passing (AMP) algorithm – an unconventional form of loopy belief propagation, was adopted to perform soft signal estimation and support detection with a computational complexity that is linear in all problem dimensions [18].

3. CLS IMAGING SYSTEM THROUGH SCATTERING MEDIUM

3.1. CLS imaging system architecture

The CLS imaging system can be conceptualized as a "coding" machine (Figure 2). During image acquisition, entries from a codebook {A} (i.e., a measurement pattern A_i) sequentially encode the target. During image reconstruction, the encoder output {Y} and an *appropriate* codebook {Φ} can used to recover the target scene. Here the purposely different notation Φ indicates that the encoder and decoder may require *different* codebooks when imaging through the scattering medium.

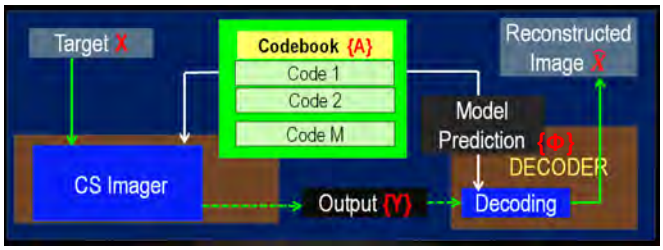

Figure 2. CLS System as a Coding Machine

The CLS illuminator shares some similarity with the streak tube imaging Lidar [15]. Nevertheless, instead of one-dimensional (1D) fan beam, a laser source modulates the digital micromirror device DMD and projects a series of 1D *"fan" patterns* onto the current target line (Figure 3). Each pattern corresponds to one row in the CS measurement matrix (i.e., codebook). At the receiver, similar to the LLS system, a single element receiver such as the photomultiplier tube (PMT) records the total photon reflection corresponding to the modulation of the spatial pattern with the target as the

measurement. Each line is measured *independently*; the platform motion enables the sensing of the target scene in line-by-line fashion.

In the CLS system, resource compression is achieved by reducing the required measurements per line while still maintain desired image quality.

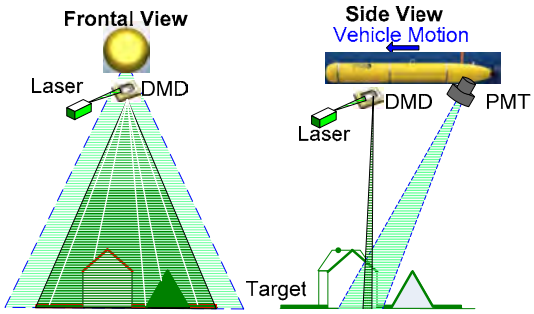

Figure 3. CLS Imaging system architecture

3.2. CLS Signal Model

For the CLS system operating in the scattering medium, such as in the underwater environment, when a binary pattern of highly collimated light is emitted from the transmitter, the light will diffuse and attenuate as it propagates to the target. The degree of spreading/attenuation is determined by the laser beam divergence, target range, and the inherent optical properties of the water. Assuming a wide receiver aperture and Lambertian reflection at the scene, the total photon flux corresponding to the m^{th} measurement Y can be represented by the equation:

$$Y_m(r+\Delta r_m) = P_{sys}\frac{\alpha_{TR}}{N_{1,m}}\left(\sum_{j=-U}^{U}\sum_{i=1}^{N}\left[\underbrace{\left(BSF_{IT}(i,j) * A_m(i,j)\right)}_{\Phi_m} \circ X(i, r+\Delta r_m - j)\right] + \hat{\beta}_m\right) \tag{5}$$

Where $*$ denotes convolution and $\circ$ represents the Hadamard point-by-point product, Y_m is the total reflected photon flux; r is the current line under investigation; P_{sys} is a constant accounting for the system configuration (receiver aperture, illumination power etc.); α_{TR} is an attenuation coefficient related to radiative transfer from the scene back to the sensor; $\Phi_m = A_m * BSF_{IT}$ is the measurement pattern on the target (i.e., the original binary pattern after propagating from the illuminator to the target through a scattering and absorbing medium described by the beam spread function BSF_{IT}); $\Phi_m \circ \boldsymbol{X}$ is the (information bearing) "imprinted" pattern due to the modulation of the measurement pattern by the target scene reflectance pattern; N is the number of pixels within each line; $N_{1,m}$ is the number of 'on' pixels in the illumination pattern m; U is the effective vertical aperture due to the spreading in the vertical (along track) direction; $\Delta L_m = mv\Delta t$ is the platform displacement when the measurement pattern m is projected (relative to the previous pattern); Δt is the refresh time of the spatial light modulator (SLM) device and v is the platform speed.

We will make two reasonable approximations: 1) the SLM refresh rate is sufficient fast relative to the platform speed; and 2) the beam spread function has a separable kernel that can be decomposed into: $BSF_{IT} \approx B^H B^V$, where B^V and B^H describe the vertical and horizontal beam spreading respectively. Taking into consideration that A_m is now a 1D pattern, Equation (5) can be simplified to:

$$Y_m(r) \approx P_{sys}\frac{\alpha_{TR}}{N_{1,m}}\left(\sum_{j=-U}^{U} B^V(j) \circ \left(\sum_{i=1}^{N} \Phi_m^H(L,i) \circ X(i, r-j)\right) + \hat{\beta}_m\right) \tag{6}$$

4. NEW CLS SOLVER BASED ON THE INTEGRATION OF DCS[a] AND DCS[b]

4.1. DCS[a] JSM-1 based CLS Solver

In the current CLS framework, the aforementioned DCS[a] JSM-1 is adopted. The predicted measurement matrix is used to recover a group of lines jointly. The corresponding CS cost function then becomes:

$$\tilde{\boldsymbol{\alpha}}^{*} = \arg\min \|\boldsymbol{a}_c\|_1 + \|\boldsymbol{a}_1\|_1 + \cdots + \|\boldsymbol{a}_L\|_1 \quad \text{subject to } \|Y - \hat{\Phi}\,\Psi\boldsymbol{a}\|_2 \le \mathcal{E}, \quad X = \Psi\boldsymbol{a} \ge \mathbf{0} \tag{7}$$

where L is the group of lines to be solved jointly. Compared to Equation (1), Equation (7) also incorporates a non-negative constraint. In order to comply with the DCS[a] measurement matrix formation in Equation (1), we introduce another approximation, ignoring the vertical spreading:

$$\hat{\Phi} \approx \Phi_m^H = B^H * A_m(r) \tag{8}$$

The corresponding process is illustrated in the flow chart in Figure 4.

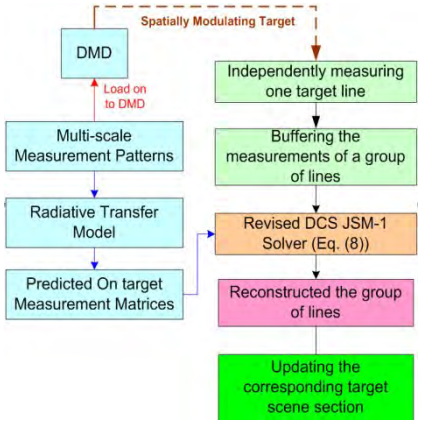

Figure 4. CLS System processing flow

One unique feature of this framework is that it shares some similarity with the "lucky imaging" scheme. As illustrated in Equation (9), assuming the current line group parameter $L > 1$, then the reconstruction of line r will be included in L solutions:

$$\begin{aligned}
&\tilde{\boldsymbol{\alpha}}_*^{\mathbf{1}} = \arg\min \|\boldsymbol{a}_c^{\mathbf{1}}\|_1 + \|\boldsymbol{a}_{L-r}\|_1 + \cdots + \|\boldsymbol{a}_r\|_1, \quad \text{subject to } \|Y_{L-r}^{r} - \hat{\Phi}\,\Psi\boldsymbol{a}\|_2 \le \mathcal{E}, X^1 = \Psi\boldsymbol{a}^{\mathbf{1}} \ge \mathbf{0} \\
&\tilde{\boldsymbol{\alpha}}_*^{\mathbf{2}} = \arg\min \|\boldsymbol{a}_c^{\mathbf{2}}\|_1 + \|\boldsymbol{a}_{L-r+1}\|_1 + \cdots \|\boldsymbol{a}_r\| + \|\boldsymbol{a}_{r+1}\|_1, \quad \text{subject to } \|Y_{L-r+1}^{r+1} - \hat{\Phi}\,\Psi\boldsymbol{a}\|_2 \le \mathcal{E}, X^2 = \Psi\boldsymbol{a}^{\mathbf{2}} \ge \mathbf{0} \\
&\quad \cdots \\
&\tilde{\boldsymbol{\alpha}}_*^{\boldsymbol{L}} = \arg\min \|\boldsymbol{a}_c^{\boldsymbol{L}}\|_1 + \|\boldsymbol{a}_r\|_1 + \cdots \|\boldsymbol{a}_r\| + \|\boldsymbol{a}_{r+L}\|_1, \quad \text{subject to } \|Y_r^{r+L} - \hat{\Phi}\,\Psi\boldsymbol{a}\|_2 \le \mathcal{E}, X^L = \Psi\boldsymbol{a}^{L} \ge \mathbf{0}
\end{aligned} \tag{9}$$

We will buffer these L solutions and the optimum reconstruction for line r can then be derived from these L solutions. One straightforward approach is to apply filtering such as a median filter to obtain the final solution:

$$\boldsymbol{a}_r^{\boldsymbol{o}} = median[\boldsymbol{a}_r^{\boldsymbol{u}}], \quad \text{for } u = 1 \ldots L \tag{10}$$

While this framework has been validated through application to test-tank experiment datasets acquired at different turbidity cycles (Figure 5) [3], the image quality at higher turbidities (Figure 5b and 5c) leaves much room for improvement.

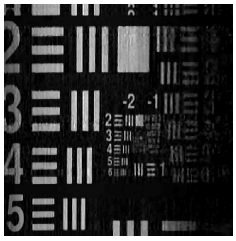

(a) Clearwater

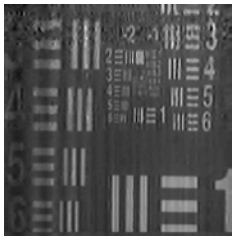

(b) C=0.6 (3 attenuation length)

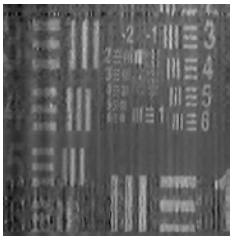

(c) C=0.8 (4 attenuation length)

Figure 5. Reconstructed image at 2:1 compression using test tank experimental data (Clearwater dataset acquired on 9/20/2013, two turbidity cycle datasets acquired on 4/29/2014. Two different optical front end configurations were used in these two experiments) [3]

The deficiency in the illuminator optical front end of the prototype system is one of two factors impacting image quality [3]. On the algorithm side, as shown in Equation (6), the measurements of every line are affected by the adjacent lines and pixels (i.e., forward scattering), and the non-information bearing backscattering photons. While the forward scattering among the adjacent pixels within the same line were addressed in Equation (7), the contribution from the adjacent lines is problematic. The forward scattering from the adjacent lines essentially means that the underlying process is non-causal since the measurements for the current line contain information from the previous lines (i.e., past)

and the subsequent lines (i.e., future). The DCS[a] framework (Equation 1) describes a memoryless system, which is the need for the approximation in Equation (8). With regard to backscattering mitigation, although the polarity flipping technique was shown to be helpful [1], the impact from the backscattering remained prominent, in Figure 5b and 5c.

While there certainly is a need to improve the prototype system hardware, we will focus on enhancing image quality by improving the algorithm.

4.2. Proposed CLS Reconstruction Technique through the Integration of DCS[a] and DCS[b]

From the compressive sensing perspective, the effect of the backscattering and forward scattering interference is reduced signal sparsity via more information injected the measurements. On the other hand, the main theme in the DCS[b] school of thought is to use a priori information to improve signal sparsity when recursively solving a time sequence of signals. Additionally, both causal filtering and non-causal smoothing can be easily realized in DCS[b], overcoming one limitation in the current CLS solver. Therefore, the proposed new design attempts to better mitigate the interferences from backscattering and forward scattering through the integration of the DCS[b] concept into the current DCS[a] based framework.

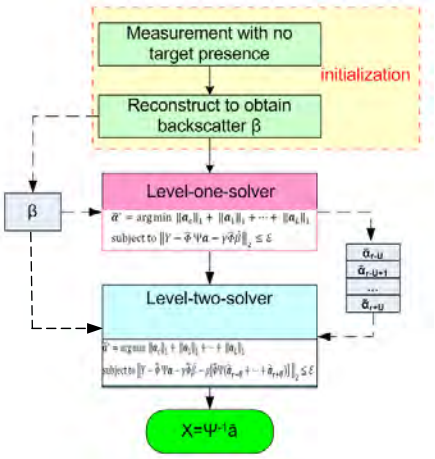

Figure 6. Flow chart illustrates the proposed CLS reconstruction algorithm

The flow chart in Figure 6 outlines the proposed two-stepped solution. The new technique consists of three phases. We start with the reasonable assumption that the imaging system will first traverse through regions with no target presence to perform the initialization, allowing us to measure the contribution of the volume backscatter $\hat{\beta}$. We assume the volume backscatter to be invariant with the same system configuration and environment conditions (i.e., same IOPs). We then proceed to invoke the Level-one-solver:

$$\tilde{\boldsymbol{\alpha}}^{*} = \arg\min \|\boldsymbol{a}_c\|_1 + \|\boldsymbol{a}_1\|_1 + \cdots + \|\boldsymbol{a}_L\|_1$$
$$\text{subject to } \left\|Y - \hat{\Phi}\,\Psi\boldsymbol{a} - \gamma\hat{\Phi}\hat{\beta}\right\|_2 \le \mathcal{E},\ \mathrm{X} = \Psi\mathrm{a} \ge 0 \qquad (11)$$

where γ is a weighting constant. Comparing Equations (7) and (11), this step is essentially the original DCS[a] based solver adjusted for the contribution of the backscattering assessed prior to the measurements. The more significant aspect of the proposed technique is that it also incorporates the Level-two-solver, which becomes involved after the current line is outside the effective vertical aperture. Consequently, the solution incorporates contributions to the measurements from the adjacent lines obtained in Level-one in addition to the backscatter:

$$\tilde{\boldsymbol{\alpha}}_{\boldsymbol{p}}^{*} = \arg\min \|\boldsymbol{a}_c\|_1 + \|\boldsymbol{a}_1\|_1 + \cdots + \|\boldsymbol{a}_L\|_1$$
$$\text{subject to } \left\|Y - \hat{\Phi}\,\Psi\boldsymbol{a} - \gamma\hat{\Phi}\hat{\beta} - \mu\left[\hat{\Phi}\Psi(\tilde{\boldsymbol{\alpha}}_{\boldsymbol{r-U}}^{\boldsymbol{l1}} + \cdots + \tilde{\boldsymbol{\alpha}}_{\boldsymbol{r}}^{\boldsymbol{l1}} + \cdots + \tilde{\boldsymbol{\alpha}}_{\boldsymbol{r+U}}^{\boldsymbol{l1}})\right]\right\|_2 \le \mathcal{E},\ X = \Psi a \ge 0 \qquad (12)$$
$$\tilde{\boldsymbol{\alpha}}_{\boldsymbol{r}} = \mu\tilde{\boldsymbol{\alpha}}_{\boldsymbol{r}}^{\boldsymbol{l1}} + \tilde{\boldsymbol{\alpha}}_{\boldsymbol{p}}$$

where γ and μ are two weighting constants, $\tilde{\boldsymbol{\alpha}}_{\boldsymbol{i}}^{\boldsymbol{l1}}, \boldsymbol{i} = \boldsymbol{r} - \boldsymbol{U} \ldots, \boldsymbol{r}, \ldots \boldsymbol{r} + \boldsymbol{U}$ are the solutions from the Level-one-solver. Equation 12 shares strong similarity with the modified-CS-residual in Equation 3. The two main differences are:1) The solver is based on DCS[a] and 2) In the final solution, we annihilate the terms corresponding to the backscatter and forward scattering from adjacent lines estimated in the Level-one-solver.

5. EXPERIMENTAL RESULTS

We now present the results of applying the new algorithm to the same dataset that produced the images in Figure 5. We first briefly describe the prototype systems and the experimental setup. [3].

5.1. Prototype System Architecture and Experimental Setup

The overall system consists of the illumination and the receiver subsystems (Figure 7a). The configuration of the receiver consists of a Hamamatsu R9880U-210 PMT with 12 degree field of view. The core of the illumination subsystem is a compact DLP Lightcrafter evaluation module, consisting of a DMD with an array of 608 x 684 pixels.

The validation tests were conducted in the FAU Harbor Branch optical test tank (Figure 7b). A linear drive mounted against the catwalk provides both vertical and lateral translation. The linear drive motion accuracy is +/-0.5 mm. The catwalk itself can be manually moved to provide an additional degree of freedom. During the experiment a 75cm^2 USAF1952-B target (Figure 6d) was attached to the linear drive and placed 5m away from the view port (Figure 7c). A Matlab program was developed to synchronize the linear drive movement, the data acquisition and the pattern cycling on the Lightcrafter. During the experiments, the linear drive moved at 1.5mm increment. The NI-6133 data acquisition board operated at 80KHz sampling rate. Each data acquisition was triggered by the Lightcrafter trigger output. Four hundred points were acquired for each pattern, and the average of these 400 points was recorded as the corresponding measurement. While the Lightcrafter is capable of a 4KHz refresh rate in the binary "pattern sequencing" mode, the Lightcrafter was operated at a 400Hz refresh rate to ensure sync stability during all the tests.

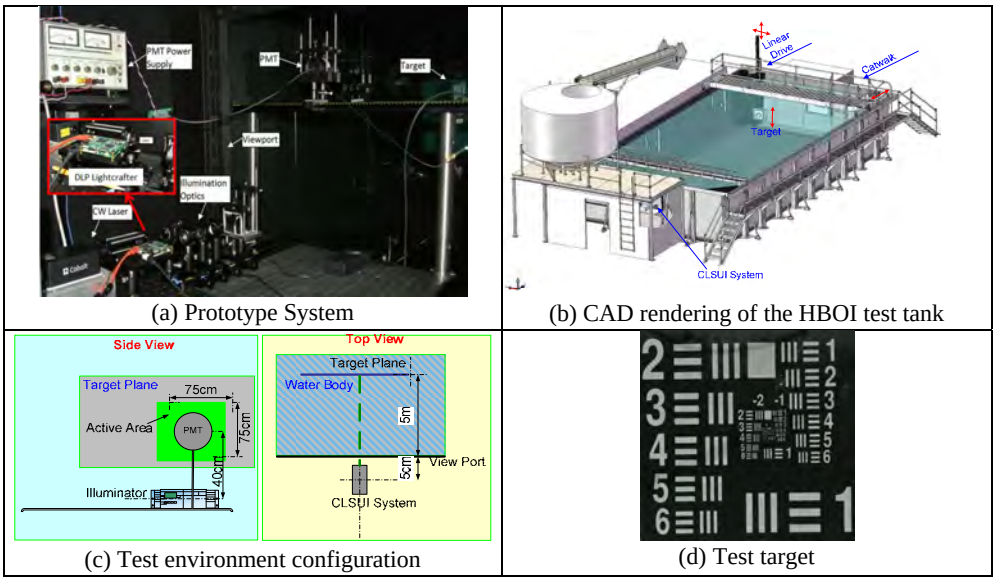

(a) Prototype System

(b) CAD rendering of the HBOI test tank

(c) Test environment configuration

(d) Test target

Figure 7 Illustration of the prototype system, the FAU Harbor Branch Optical Imaging Test Tank and the test setup configuration

For image quality evaluation, we will adopt the anisotropy based blind image quality assessment metric: Anisotropic Quality Index (AQI) proposed in [19]. AQI computes the variance of the expected entropy of a given image as a function of the directionality, which is taken as an anisotropy indicator. Experiments results in [19] show this metric presents some desirable features that resemble those from an ideal image quality function, constituting a suitable quality index to assess both the contrast and resolution of natural images. AQI produces a score between 0 and 1, with 1 being the higher score indicates better image quality/fidelity.

5.2. Clear Water Experiments

We first apply the proposed technique to the clear water dataset obtained on 9/18/2013 [3]. Using a projection path beam concentration optical front end [3], the achievable horizontal image resolution was 512 pixels/line. For this dataset, the two constants in Equation (12) were: γ=0.25 and μ=0.25. The comparison of the performance of the proposed technique with the original DCS[a] based approach using the clear water dataset are shown in Figure 8. The proposed technique achieves two improvements over the original DCS[a] based approach: the image contrast is improved due to the reduction of the noise in the black regions, and a better image resolution is apparent. These are more evident by comparing the

high resolution regions of the target, marked on Figure 8a and 8d. Figure 8 illustrates the performance at several different compression ratios (CRs). The image contrast and resolution improvement can be observed at all the compression ratios.

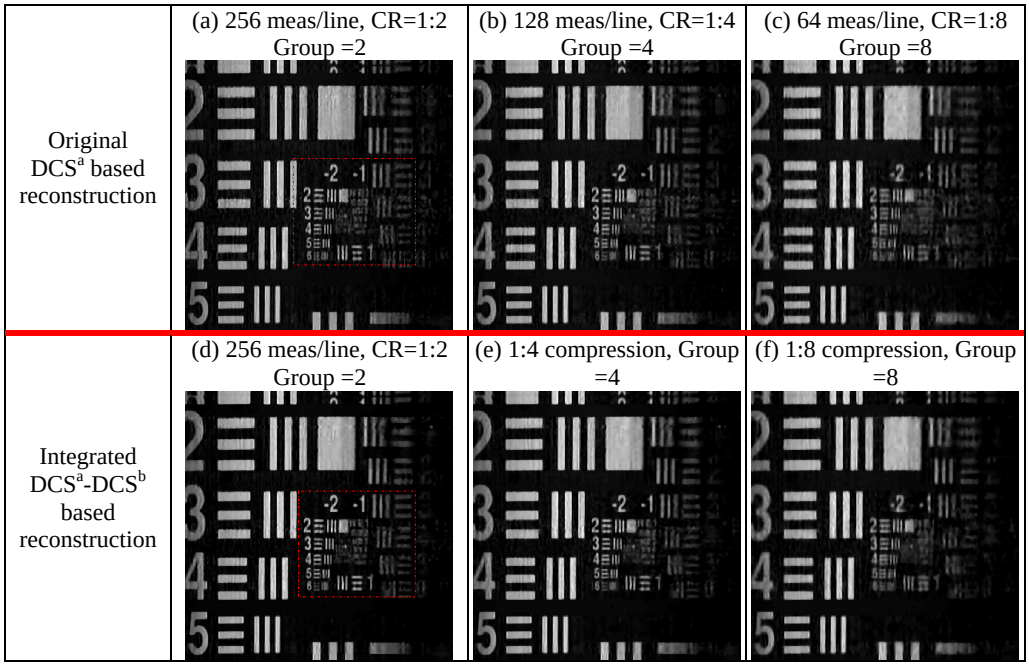

Figure 8 Comparison of the performance of the proposed technique with the original DCS[a] based approach using the clear water dataset at different compression ratios

The AIQ scores in Figure 9 reinforce the visual observation from Figure 8. Interestingly, the integrated technique produced a higher AIQ score at CR=8:1 than the AIQ score at CR=4:1 achieved using the original DCS[a] technique.

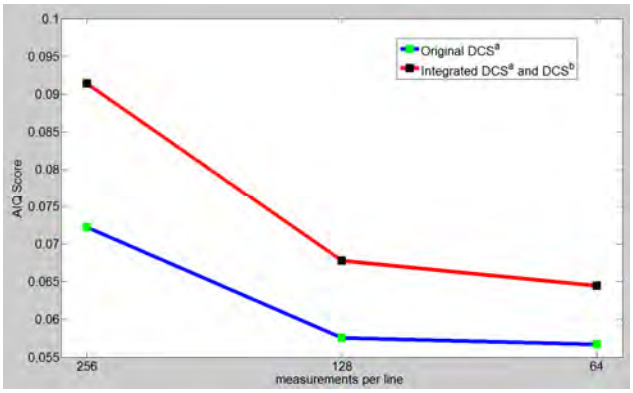

Figure 9 Comparison of the AIQ metric of the proposed technique with the original DCS[a] based approach against the clear water dataset at different compression ratios

5.3. Turbidity cycle tests

We also apply the technique to the turbidity cycle dataset acquired on 4/28/2014. During this test, a different illuminator design that focuses the beam along the illumination path was adopted [3], to increase the system power output. The cost of this method is reduced optical front end robustness against external vibrations during the measurement phase, which yielded the more noisy regions on the images shown in the following figures. The achievable horizontal resolution is 448 pixels/line.

Figure 10 compares the results of the two techniques at C=0.6 (3 attenuation lengths) at three different compression ratios. The two constants in Equation (12) were: γ=0.6 and μ=0.5.

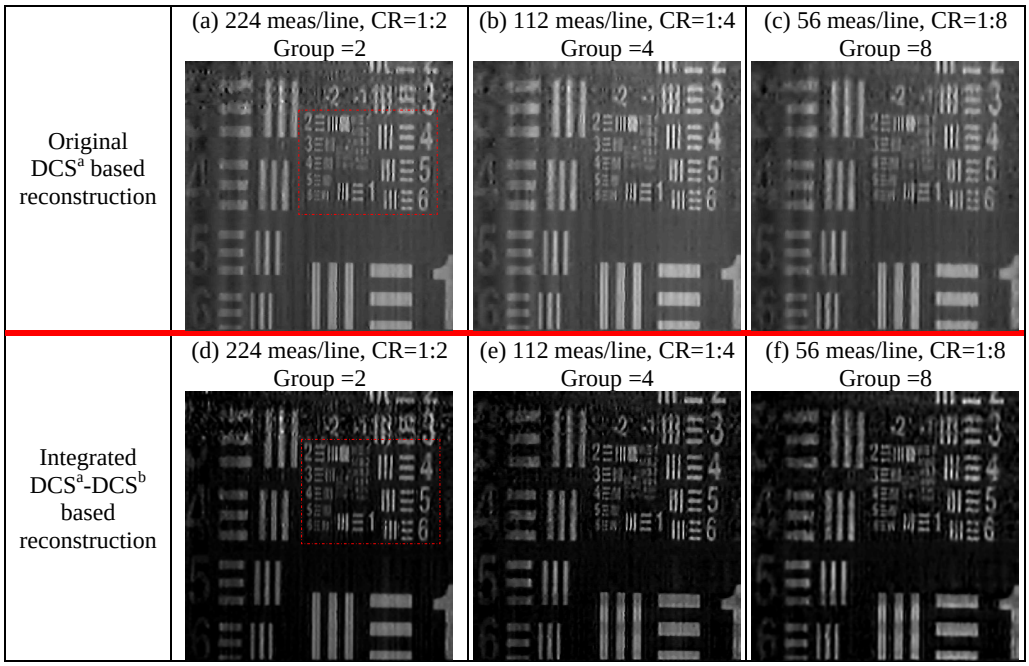

Figure 10. Comparison of the performance of the proposed technique with the original DCS[a] based approach using the test dataset with C=0.6, 3 attenuation lengths, at different compression ratios

The proposed technique again produced both contrast and resolution improvements at different compression ratios. The resolution improvements were more evident in the marked high-resolution regions in Figure 10. Such improvement is again reinforced from the corresponding AIQ scores in Figure 11 below.

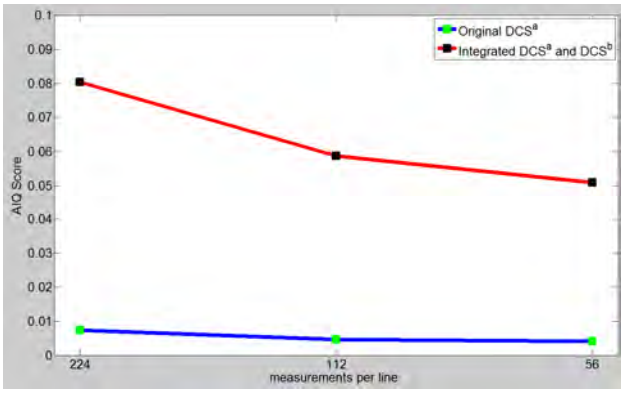

Figure 11 Comparison of the AIQ metric of the proposed technique with the original DCS[a] based approach against the dataset with C=0.6, 3 attenuation lengths, at different compression ratios

Figure 12 compares the results of the two techniques at C=0.8 (4 attenuation lengths). The two constants in Equation (12) are: γ=0.9 and μ=0.5. As with the case of C=0.6, the image contrast and resolution improvements can be observed at all the compression ratios.

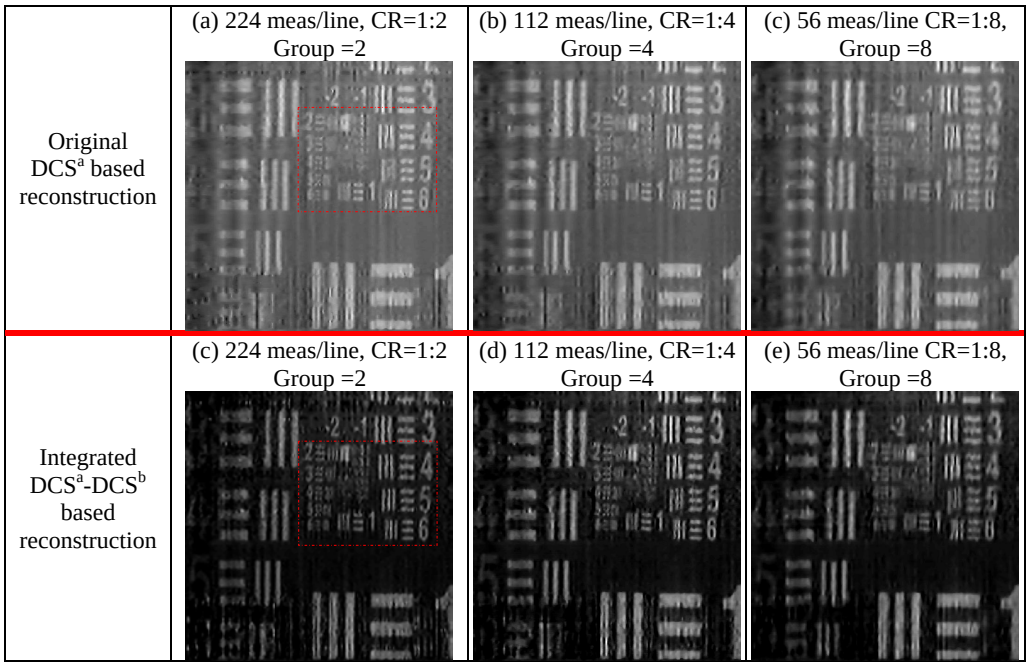

Figure 12. Comparison of the performance of the proposed technique with the original DCS[a] based approach at different compression ratios, (C=0.8, 4 attenuation lengths)

The AIQ scores in Figure 13 below confirm the visual observations based on Figure 12.

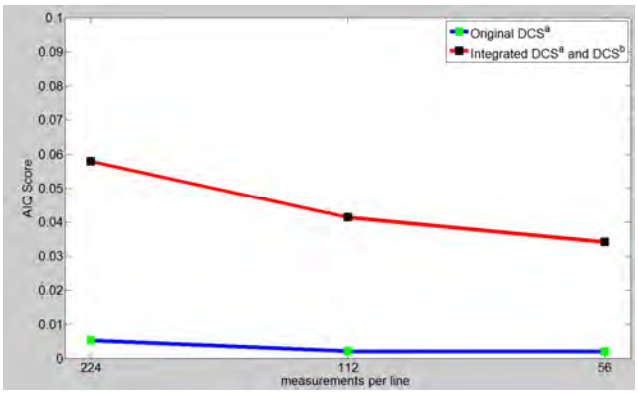

Figure 13 Comparison of the AIQ metric of the proposed technique with the original DCS[a] based approach against the dataset with C=0.8, 4 attenuation lengths, at different compression ratios

6. CONCLUSIONS

This paper describes a new reconstruction technique for a previously proposed compressive line sensing underwater imaging system [1]. One deficiency in the existing CLS reconstruction framework is that the interferences from the volume backscatter and the forward scattering from the adjacent lines are not adequately mitigated. The core idea in the proposed technique is to incorporate the Bayesian inference based dynamic compressive sensing approach into the original "memoryless" distributed compressive sensing framework. The non-causal reconstruction framework resulted from such integration enables us to better mitigate the aforementioned issues, resulted in the improved image contrast and resolution. The effectiveness of the technique was validated using data acquired in the experiments conducted in the FAU Harbor Branch optical test tank.

One feature of the CLS imager as a "coding machine" is that there is a certain level of disjoint between the hardware-dependent measurement acquisition (i.e., encoding) process and the image reconstruction (i.e., decoding) process. The work described here reveals a benefit of such separation. With the same data acquisition hardware, it is possible to enhance the system performance through algorithm improvement. Such adaptive underlying architecture and the algorithm-centric implementation can potentially reduce innovation and enhancement costs. Although a more robust prototype system should certainly improve the performance as well. The deficiencies of the prototype system provided an opportunity to demonstrate the ability of the CLS imager to "self-repair" a hardware limitation through cost function adaptation.

The proposed technique assumes a static environment (i.e., time invariant point spread function). It therefore will be interesting to study how to further improve the proposed technique so that it can be more effective in the more challenging cases where the point spread function is time variant – such as when imaging through turbulence.

ACKNOWLEDGMENT

This work was support by 2013 AFOSR Young Investigator Program, Naval Research Lab contract N00173-15-P-0263, HBOI internal funding and TCU Invest Scholar Fund. The authors want to thank Mr. Ben Metzger for the help during all phases of the experimental tests.

REFERENCES

[1] B. Ouyang, F. R. Dalgleish, F. M. Caimi, T. E. Giddings, W. Britton, A. K. Vuorenkoski, and G. Nootz, "Compressive Line Sensing Underwater Imaging System", SPIE Optical Engineering Vol. 53, Issue 5, April 2014.

[2] B. Ouyang, F. R. Dalgleish, F. M. Caimi, T. E. Giddings, J. J. Shirron, A. K. Vuorenkoski., G. Nootz, W. Britton and B. Ramos, "Compressive Sensing Underwater Laser Serial Imaging System", Journal of Electronic Imaging, special edition on Compressive Sensing, Vol. 22, Issue 2, 2013.

[3] B. Ouyang, F. M. Caimi, F. R. Dalgleish, A. K. Vuorenkoski and W. Hou, "Experimental studies of the compressive line sensing underwater serial imaging system", SPIE Proceedings Vol. 9111, 2014.

[4] D. Baron, M. B. Wakin, M. F. Duarte, S. Sarvotham, and R. G. Baraniuk, "Distributed compressed sensing", Rice University, Depart. Electrical and Computer Engineering Technical Report TREE-0612, Nov 2006.

[5] E. Candes, J. Romberg, and T. Tao, "Stable Signal Recovery from Incomplete and Inaccurate Measurements," Comm. Pure Appl. Math., vol. 59, pp. 1207-1223, 2006.

[6] F. R. Dalgleish and F. M. Caimi, "Synchronous Laser Line Scanners for Undersea Imaging Applications," Accepted as a book chapter for Taylor and Francis series in Optical Engineering (Laser and Optical Scanning).

[7] F. R. Dalgleish, B. Ouyang, A. K. Vuorenkoski, B. Metzger, B. Ramos and W R. Britton, "Extended range distributed laser serial imaging in turbid estuarine and coastal conditions," Proc. MTS/IEEE Oceans'12, 2012.

[8] F. R. Dalgleish, A. K. Vuorenkoski and B. Ouyang, "Extended-Range Undersea Laser Imaging: Current Research Status and a Glimpse at Future Technologies", Marine Technology Society Journal, 47(5):128-147, 09/2013.

[9] D. Donoho, "Compressive Sensing," IEEE Trans. Inform. Theory, vol. 52, pp. 1289-1306, 2006.

[10] D. Dudley, W. Duncan and J. Slaughter, "Emerging Digital Micromirror Device (DMD) Applications," Proc of SPIE, 2003, 4985, 14-25.

[11] S. Q. Duntley, R. W. Austin, R. L. Ensminger, T. J. Petzold, and R. C. Smith, "Experimental TVI System Report," Visib. Lab. Tech. Rep., pp. 74–1, 1974.

[12] T. E. Giddings and J. J. Shirron, "Numerical Simulation of the Incoherent Electro-optical Imaging Process in Plane-Stratified Media," Opt. Eng. vol. 48, no. 12, 126001 (2009).

[13] T. J. Kulp, D. Garvis, R. Kennedy, T. Salmon, K. G. Cooper, "Development and testing of a synchronous-scanning underwater imaging system capable of rapid two-dimensional frame imaging,", Appl. Opt. Jul 1;32(19):3520-30, 1993.

[14] W. Lu, T. Li, I. Atkinson and N. Vaswani, "Modified-CS-Residual for Recursive Reconstruction of Highly Undersampled Functional MRI Sequences", IEEE Intl. Conf. Image Proc. (ICIP) 2011.

[15] B. C. Redman, A. J. Griffis, and E. B. Schibley, "Streak Tube Imaging Lidar (STIL) for 3-D Imaging of Terrestrial Targets," Proc. of 2000 Meeting of the MSS Specialty Group on Active E-O Systems, 11–13, 2000.

[16] D. Slepian and J. K. Wolf, "Noiseless coding of correlated information sources", IEEE Trans. Inform. Theory, vol. 19, pp. 471–480, July 1973.

[17] A. D. Wyner and J. Ziv, “The rate-distortion function for source coding with side information at the decoder”, IEEE Transactions on Information Theory, Jan, 1976.
[18] J. Ziniel, P. Schniter, “Dynamic compressive sensing of time-varying signals via approximate message passing”, IEEE Transactions on Signal Processing 61 (21), 5270-5284, 2013.
[19] S. Gabarda and G. Cristóbal, “Blind image quality assessment through anisotropy”, J. Opt. Soc. Am. A/ Vol. 24, No. 12, pp. B42-B51, 2007.